THE DIRAC R-MATRIX METHOD FOR SCATTERING OF SLOW ELECTRONS FROM ALKALI-METAL-LIKE TARGETS

Uwe Thumm
Department of Physics, Kansas State University, Manhattan, KS 66506-2601 USA

ABSTRACT

The Dirac R-matrix theory is a close-coupling method that includes a fully relativistic representation of the target. We outline this method for the interaction of slow incident electrons with (effectively) one-electron, alkali-metal-like targets. Our numerical results for atomic cesium targets include total, angle-differential, and momentum-transfer scattering cross sections, spin-polarization parameters, and light-polarization parameters for the radiative decay of impact-excited target states. We discuss the influence of induced core polarization and relativistic effects on the lowest bound and resonant states of Cs^-.

1. INTRODUCTION

Being rather simple one-electron-like systems, alkali-like targets are an attractive subject for the study of their interactions with slow incident electrons.Theoretically, these relatively uncomplicated systems are accessible to an effective-potential description which reduces the dynamics of the multi-electron targets to the motion of a valence electron in a suitably chosen model potential for the noble-gas-like core. Over the years, such models turned out to be very successful in describing low-energy electron-impact phenomena on the condition that the effective core potentials are carefully matched to the lower part of the target spectrum [1, 2].

Heavy alkali-like targets can be used to investigate relativistic effects. Cesium, in particular, appears to be a good candidate for a detailed study of spin-, fine-structure-, or hyperfine-structure dependent effects; it is relatively easily accessible in the laboratory, has a long record of experimental investigations spanning more than 60 years [1, 3], is of some technological interest [3] and has been presented in several calculations [1]–[15]. Nevertheless, the electron-Cs collision system is a subject of speculation, in particular about the existence of low-lying resonances in the elastic scattering cross section [1] that had previously been identified as bound excited states of Cs^- [2, 10, 11, 16].

In this contribution, we first outline our formulation [1] of the Dirac R-matrix method [7] for the effective three-body system formed by two active electrons (the incident and the valence electron) and a relatively inert, but polarizable, noble-gas-like core (section 2). This non-perturbative method provides access to three-body bound states, as well as to the complete description of the scattering process with possibly spin-polarized collision partners. We then discuss our numerical results [1, 3, 13, 15] for atomic Cs targets and incident electrons with less than 3 eV kinetic energy in comparison with available experimental and theoretical data (section 3). Unless otherwise stated, we use atomic units.

2. THE DIRAC R-MATRIX METHOD FOR ALKALI-LIKE TARGETS

The key feature of the R-matrix theory is a division of configuration space into two (or more) subspaces in which the many-particle problem is treated at different levels of approximation. Introducing a sphere of radius ρ, large enough to accommodate the target in its ground and lowest excited states, we shall first treat the inner and outer regions separately and then combine the two in formulating the matching condition for the two-electron wave function at the surface of the 'R-matrix sphere'. The solution of the matching equation contains the complete information of the scattering event, is easily related to measurable quantities, and allows us to determine the affinities of bound states of the effective three-body system.

In the inner region ($r < \rho$), we solve the two-electron problem at a rather high level of approximation and include all one-electron relativistic effects, exchange, and the dielectronic response of the core to the two active electrons. We split the full Hamiltonian

$$H = H_1 + H_2 + H_{12} \tag{1a}$$

into one-electron Dirac Hamiltonians

$$H_k = c\sum_{i=1}^{3} \alpha_i p_{ki} + (\beta - 1)c^2 + V_{core}(r_k), \tag{1b}$$

that describe the interaction of each outer electron with the core through the adjustable potential

$$V_{core}(r) = V_{TFDA}(\lambda, r) + V_{pol}(\alpha_d, \alpha_q, \bar{r}_c, r) \tag{2a}$$

$$V_{pol} = -\frac{\alpha_d}{r^4}\, W_6(\bar{r}_c, r) - \frac{\alpha_q}{r^6}\, W_{10}(\bar{r}_c, r) \tag{2b}$$

$$W_n = 1 - \exp\left[-(r/\bar{r}_c)^n\right], \tag{2c}$$

and the interaction

$$H_{12} = \frac{1}{r_{12}} + V_{diel}(r_c, \vec{r}_1, \vec{r}_2) \tag{3a}$$

$$V_{diel} = -\frac{\alpha_d}{r_1^2 r_2^2}\, [W_6(r_c, r_1)\, W_6(r_c, r_2)]^{1/2}\; P_1(\cos\theta_{12}) - \frac{\alpha_q}{r_1^3 r_2^3}\, [W_{10}(r_c, r_1)\, W_{10}(r_c, r_2)]^{1/2}\; P_2(\cos\theta_{12})\,. \tag{3b}$$

The scaling parameter λ in the Thomas-Fermi-Dirac-Amaldi potential V_{TFDA}, the static dipole and quadrupole polarizabilities α_d and α_q, and the cut-off radius $\bar{r}_c$ of the induced core-polarization potential V_{core} are determined by fitting the target spectrum such that the eigenvalues of H_k reproduce the lowest energy levels of the target.

Apart from the Coulomb repulsion, the interaction H_{12} between the two active electrons is determined by the 'dielectronic term' V_{diel}, which adds the influence of the core polarization caused by one active electron on the motion of the other active electron. P_l are Legendre polynomials and θ_{12} is the angle between the radius vectors $\vec{r}_1$ and $\vec{r}_2$ of both electrons. The cut-off radius r_c in V_{diel} is used to 'gauge' the two-electron spectrum. For atomic alkali targets, r_c is obtained by matching the lowest eigenvalue of H to the (well known) electron affinity of the negative ion in its stable ground state.

By diagonalizing H (inside the R-matrix sphere) we obtain eigenvalues E_K and coefficients of the eigenfunctions

$$\Psi_K(\vec{r}_1,\vec{r}_2) = \sum_{ij} c_{ijK} \left[\phi_i^b(\vec{r}_1)\,\phi_{ij}^c(\vec{r}_2)\right] + \sum_{ii'} d_{ii'K} \left[\phi_i^b(\vec{r}_1)\,\phi_{i'}^b(\vec{r}_2)\right] , \; r_{1,2} \le \rho \qquad (4)$$

with respect to a basis of antisymmetrized (symbol) products of bound and continuum orbitals, ϕ^b and ϕ^c. Typically (for sufficiently low impact energies), only a small number of bound orbitals is needed in order to represent the valence electron in the ground and lowest excited states, in accord with the basic idea of a close-coupling ansatz. The bound orbitals are eigenfunctions of (1b) with the usual boundary conditions (they practically vanish at $r = \rho$). The Dirac-R-matrix theory requires the large and small radial components, $p^c(r)$ and $q^c(r)$, of ϕ^c to satisfy unphysical boundary conditions at $r = \rho$,

$$\frac{q^c}{p^c}\,|_{r=\rho} = \frac{b+k}{2\rho c} , \qquad (5)$$

where $k = \pm(j+1/2)$ for $j = \ell \mp 1/2$ depends on the orbital angular momentum ℓ and the coupling of electron spin and ℓ to j. In the nonrelativistic limit (velocity of light = c $\to \infty$) and for our choice $b = 0$, Eqn.(5) becomes identical to the logarithmic derivative of p^c.

The Dirac R-matrix is essentally a multi-channel and relativistic generalization of the logarithmic derivative. It contains in compact form information on the dynamics of the two active electrons inside the R-matrix sphere. In terms of the surface amplitudes W_{iK} with the large component p_{ij}^c of the jth continuum orbital in channel i, the R-matrix elements are

$$R_{ii'} = \frac{1}{2\rho} \sum_K \frac{W_{iK} W_{i'K}}{E_K - E} , \qquad W_{iK} = \sum_j c_{ijK}\; p_{ij}^c(\rho) , \qquad (6)$$

where E is the total energy and where each channel i is given by a specific electronic state of the target, the quantum number k of the scattered electron, and the total angular momentum JM_J of the two-electron system [1, 7].

For all practical applications only a finite number of continuum states ϕ_{ij}^c can be retained. This incompleteness with respect to the representation of the scattered electron inside the R-matrix sphere needs to be corrected. This is conveniently and with sufficient precision accomplished by adding the so-called 'Buttle correction' to the diagonal elements of the R-matrix [1].

In the outer region ($r > \rho$), exchange can be neglected (for large enough ρ), and the Dirac equation can be simplified by neglecting terms of the order $1/c^2$ (for slow incident electrons). The large radial components of the scattered-electron wavefunction then obey the coupled radial equations

$$\left[\frac{d^2}{dr^2} + 2(\epsilon_i + V)\right] p_i^c + \sum_{i'} \sum_{\lambda=1} \frac{b_{ii'}^\lambda}{r^{\lambda+1}}\; p_{i'}^c = 0 , \quad r > \rho \qquad (7)$$

where ϵ_i is the energy of the scattered electron in channel i. The monopole term V of the target potential vanishes identically for neutral targets, and p_i^c in different channels are coupled by the long-range potential of the perturbed target with multipole coefficients $a_{ii'}^\lambda$. The $a_{ii'}^\lambda$ and the diagonal centrifugal potentials are included in the

coupling matrices $b^{\lambda}_{ii'} = -2a^{\lambda}_{ii'} - \ell_i(\ell_i+1)\delta_{ii'}\delta_{\lambda 1}$, where ℓ_i is the angular momentum of the scattered electron in channel i. If N_o channels are open, each channel contains N_o independent solutions of (7), labeled by the index j. Their asymptotic behavior in open ($\epsilon_i > 0$) and closed channels ($\epsilon_i < 0$) is

$$p^{c}_{ij} \xrightarrow[r\to\infty]{} \begin{cases} \text{æ}_i^{-1/2}(\delta_{ij}\sin\phi_i + K_{ij}\cos\phi_i) & \epsilon_i > 0 \\ \tilde{K}_{ij}\exp(-|\text{æ}_i|r) & \epsilon_i < 0 \end{cases} , \tag{8}$$

where $\text{æ}_i^2 = 2\epsilon_i$. K_{ij} and $\tilde{K}_{ij}$ are elements of the 'K matrix' and its closed-channel extension, and ϕ_i is the usual phase (e.g., ϕ_i=æ$_i$ $r - \ell_i\,\pi/2$, for neutral targets).

The K matrix is related to the scattering matrix by $S = (1+iK)(1-iK)^{-1}$ as well as to the spin-dependent scattering amplitude (by a recoupling formation, see [3] for details). We determine K by solving (7) and (8) numerically and by matching inner and outer space solutions at $r = \rho$. Scattering cross sections (for not spin-polarized collision partners) are now conveniently expressed in terms of S. The partial angle-integrated cross-section matrix for transitions between channels i and i' is (in units of πa_o^2)

$$\sigma^{J\Pi}_{i\to i'} = \frac{2J+1}{4\epsilon_i(2\underline{j}_i+1)}\,|S_{ii'} - \delta_{ii'}|^2 , \tag{9}$$

where $\underline{j}_i$ is the initial angular momentum of the valence electron. Transitions between specific target states are addressed by the partial cross section $\sigma^{J\Pi}_{\underline{n}\underline{\ell}\underline{j}\to\underline{n}'\underline{\ell}'\underline{j}'}$, which is the sum of $\sigma^{J\Pi}_{i\to i'}$ over all channels i and i' that include $\underline{n}\,\underline{\ell}\,\underline{j}$ and $\underline{n}'\underline{\ell}'\underline{j}'$ as initial and final target states, respectively. Finally, as a measurable quantity, the total, angle-integrated cross section (AICS) $\sigma_{\underline{n},\underline{\ell},\underline{j}\to\underline{n}',\underline{\ell}',\underline{j}'}$ for elastic, inelastic or superelastic scattering is obtained by summing $\sigma^{J\Pi}_{\underline{n}\underline{\ell}\underline{j}\to\underline{n}'\underline{\ell}'\underline{j}'}$ over sufficiently many J and both (total) parities Π.

If all channels are closed ($N_o = 0$), the R-matrix method can still be applied [1], although this case does not describe a scattering problem. Matching of inner and outer space solutions is now only (if at all) possible for discrete values of the total energy E that correspond to bound states of H.

Apart from AICSs, quantities that are more sensitive to details of the collision dynamics, such as momentum-transfer cross sections (MTCS), angle-differential cross sections (ADCS), and spin-polarization parameters, can be expressed as bilinear products of the scattering amplitudes [3, 15, 17]. The information available in the K-matrix (or scattering amplitude) allows for a complete description of the scattering event and parallels the maximum information accessible in a 'complete scattering experiment' [17, 18].

3. APPLICATION TO ELECTRON - Cs INTERACTION

Being an alkali atom, Cs has a small (first) ionization energy (3.9 eV) that lies well below the minimal energy necessary for core excitation (12.3 eV). Therefore, for the interaction with slow electrons of incident kinetic energy clearly below the first ionization threshold, Cs satisfies the basic requirements of section 2. In addition, with a nuclear charge of Z=55, it has noticeable fine-structure splittings (70 meV for its first excited state) that, as we will see in a moment, exceed narrow resonance structures in the low-energy scattering cross section, thereby justifying a fully relativistic treatment.

Our calculation is based on an ℓ- and j- dependent fit of the parameters in V_{core} (2) to the most reliable energy levels available in the literature [1]. We included close coupling between the five lowest target states ($6s_{1/2}$, $6p_{1/2,3/2}$, $5d_{3/2,5/2}$), 24 continuum orbitals in each channel, and Buttle-corrected for the incompleteness of the basis of continuum orbitals. We found that $\rho = 40$ a.u. is sufficiently large and adjusted the remaining undetermined parameter r_c in V_{diel} (3) to the measured electron affinity of Cs^- (471.5 meV).

3.1 Low-lying ^{3}P Resonances

We start the discussion of our numerical results with two multiplets of narrow ^{3}P resonances in the elastic scattering domain [1]. Table I shows affinities E_{Aff} and widths Γ of these resonances for the three normally-ordered terms ($J = 0, 1, 2$) in each multiplet. The surprisingly dramatic influence of the dielectronic potential (3b) is easily seen by comparing the resonance positions and width with (E_{Aff}, Γ_{Aff}), and without $(E_{Aff}^{(-d)}, \Gamma^{(-d)})$ inclusion of V_{diel} in the interaction H_{12} (2). The effect of V_{diel} can be understood by the following qualitative consideration. One of the two active electrons induces a dipole in the Xe-like core, which has its negative end where the other active electron is most likely be found, due to the predominant $1/r_{12}$ repulsions in (3a). The dielectronic term therefore enhances the electronic $1/r_{12}$ repulsion and tends to shift the negative ion spectrum towards higher energies. This shift amounts to about 20-30 meV, such that the $^3P_J^o$ resonances appear in the bound spectrum of Cs^- if we neglect V_{diel}, in agreement with earlier suggestions [2, 10, 11, 16] that Cs may have *bound* excited negative-ion states. At very low scattering energies, the $^3P_J^o$ resonances strongly enhance the elastic scattering cross section (Fig. 1a). So far, the only experimental evidence that the 6s6p $^3P^o$ state of Cs^- is a resonance is indirect and based on the analysis of the perturbation of Cs Rydberg levels by ground-state Cs and on the transport properties of electrons in weakly ionized Cs vapor [19].

We find the even-parity $6p^2\ ^3P_J^e$ states to be bound with respect to the first excitation threshold of Cs, in agreement with an earlier [6] nonrelativistic calculation. We note that in a nonrelativistic approach these states are strictly uncoupled to the adjacent continuum, such that their finite autoionization widths (Table I, Fig. 1b) are entirely due to relativistic interactions.

3.2 Angle Integrated Cross Sections

For incident electrons with energies between ~0 and 2.8 eV, we obtained converged AICS for elastic scattering and target excitation to $6p_{1/2,3/2}$ and $5d_{3/2,5/2}$ final states by summing partial cross sections over the 20 lowest J^Π symmetries (Fig. 2). The $6p^2\ ^3P_J^e$ resonances in Fig. 2 are not fully resolved and appear as a spike below the first excitation threshold, whereas the high-energy tail of the 6s6p $^3P_2^o$ term explains the rise of the cross section at the lowest shown energies. We believe that the peaks in the inelastic cross sections for $6p_{1/2,3/2}$ excitation in Fig. 2a originate in a multiplet of 6p nd $^3F_J^o$ resonances [1, 3, 22].

For the displayed energies, the sum of the elastic and inelastic cross sections in Fig. 2a is practically identical with the total cross section for electron-Cs scattering (Fig. 2b), in which the final target state remains unresolved. The most striking feature in the

Table 1: Negative-ion energies and resonance positions E_{Aff} and widths Γ in meV for Cs^- with respect to the $6s_{1/2}$ threshold (for $6s6p\ ^3P^o_J$) or the $6p_{1/2}$ threshold (for $6p^2\ ^3P^e_J$). $E^{(-d)}_{Aff}$, $\Gamma^{(-d)}$ and E_{Aff}, Γ are obtained without and with the dielectronic term. Negative values indicate states not bound relative to the given threshold.

	J^π	$E^{(-d)}_{Aff}$	$\Gamma^{(-d)}$	E_{Aff}	Γ
$6s6p\ ^3P^o_J$	0^o	28.35		−1.78	0.42
	1^o	21.39		−5.56	2.43
	2^o	8.60		−12.76	9.32
$6p^2\ ^3P^e_J$	0^e	159.68	0.005	141.24	0.009
	1^e	148.02	0.19	129.71	0.15
	2^e	126.13	1.12	108.11	1.33

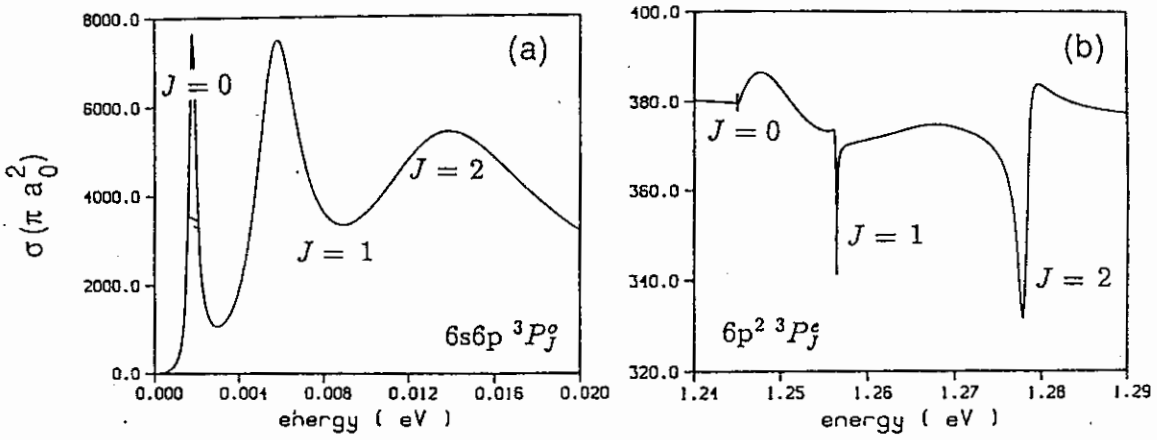

Figure 1: Angle-integrated cross sections near the $6s6p^3P^o_J$ (a) and $6p^2\ ^3P^e_J$ shape resonances.

comparison of our cross section with previous calculations is the strong $^3P^o$-resonance enhancement (Fig. 2b) . The nonrelativistic two-state calculations in Ref. [4] and Ref. [5] predict bound $^3P^o_J$ states of Cs^- which explains the lack of the resonance enhancement in the scattering cross sections (both previous calculations do not include core polarization through a dielectronic term). The more recent semirelativistic five-state calculation of Ref. [8] shows a large discrepancy with our results. This disagreement was recently [14] traced to the inappropriate use of orbitals that were derived from a trial core potential in Ref. [8]; recalculation of the orbitals in an adjusted core potential brings the results of the corrected calculation in close agreement with ours [14]. The absolute measurement of Ref. [20] has an experimental uncertainty of ± 20%, which is not quite enough to overlap our results. However, this 20-years-old investigation was a result of pioneering technology, and we therefore maintain the thought, that new absolute measurements are in order, even though a more recent experiment [21] may seem to provide evidence

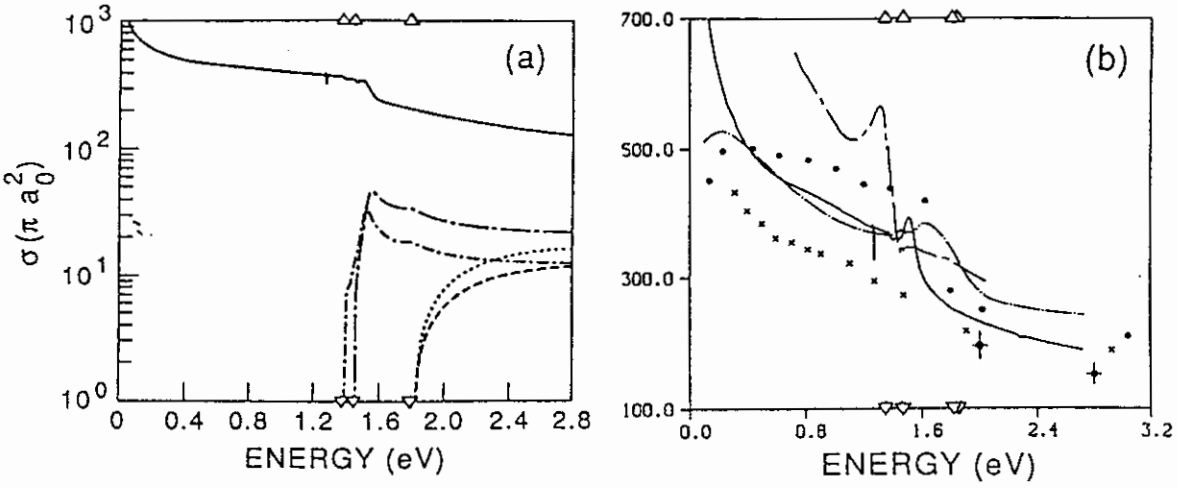

Figure 2: (a) Elastic and inelastic angle-integrated cross section. (b) Total angle-integrated cross section. Theory: present Dirac R-matrix calculation (Ref. [1]) (————), Ref. [5] (— · — · — ·), Ref. [8] (— - — -), Ref. [4] (•). Experiment: Ref. [20] (x), Ref. [21] (■). The $6p_{1/2,3/2}$ and $5d_{3/2,5/2}$ thresholds are marked by the small triangles.

that our results slightly overestimate total AICS.

3.3 Momentum-Transfer Cross Sections (MTCSs)

The MTCS is given by the integral over scattering angles θ of the ADCS weighted with the factor (1-cos θ) that is proportional to the momentum transfer during the collision. Including a higher moment of the scattering distribution, the MTCS is more sensitive to the detailed collision dynamics than the AICS. For collisions with 0.1 to 1 eV impact energy, the MTCS is of interest for the development of thermionic energy converters [3] and as an input quantity for transport calculations that attempt to predict conductivities in swarm experiments [19, 23]. Our MTCSs [3] in Fig. 3 cover the energy range of primary interest for these plasma applications and also include the immediate vicinity of the elastic threshold. Being the result of a direct close-coupling calculation, we expect them to be of higher accuracy than rather indirect methods, shown for comparison, that refer to measured thermal and electrical conductivities.

The agreement with our prediction is best for the semiempirical effective-range extrapolation [19] (below 0.1 eV) of theoretical phase shifts calculated (above 0.1 eV) in Ref. [4]. It is interesting that this extrapolation per se leads to a bound $^3P^o$ state of Cs^- and disagrees with experiment. However, the disagreement can be resolved if the polarizability of Cs as well as effective-range parameters are adjusted using experimental results for the shift and broadening of Cs Rydberg levels by Cs atoms [19]. This indirectly supports our predictions of an autoionizing $^3P^o_J$ state of Cs^- and, indeed, as shown in Fig. 3, the adjusted extrapolation of Ref. [19] produces some of the $^3P^o_J$ resonance structure.

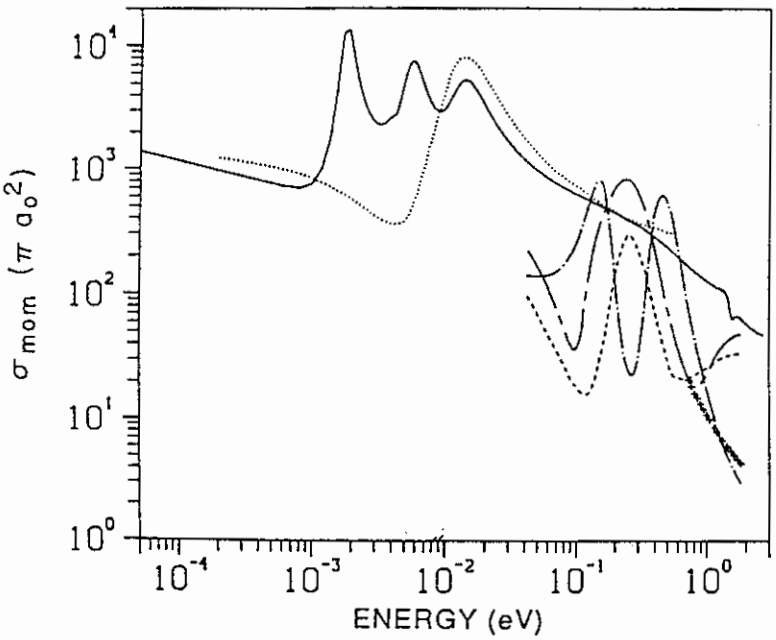

Figure 3: Momentum-transfer cross section for elastic scattering: ——— Dirac R-matrix calculation (Ref. [3]); · · · · · · Fabrikant (Ref. [24]); — · — · — · Stefanov (Ref. [23]); — - — - — Nighan and Postma (taken from Ref. [23]); - - - - - - Crown and Russek (taken from Ref. [23]); ++++++ Postma (taken from Ref. [23]).

3.4 Angle-Differential Cross Sections

Regarded as a function of θ and for fixed scattering energy E, the very-low-energy ADCS [3] shows a pronounced $\cos^2\theta$-like behavior due to dominant contributions from p-wave scattering (Fig. 4a). At E=100 meV this behavior still dominates (Fig. 4b), but loses its influence quickly as E is further increased due to strong admixture of higher partial waves. At 1 eV a local maximum appears at $\theta \approx 90°$ that can be assigned to increasingly important d-wave scattering. Regarded as a function of E and for fixed θ, we recover the three terms of the $^3P_J^o$ resonance (Fig. 4a) and a strong decline of elastic scattering at the onset of the first inelastic threshold (Fig. 4b). At energies above 1.4 eV, our elastic ADCSs are in fair agreement with the relative experimental results of Ref. [22] and also with the previous two-state calculation of Ref. [4] (Figs. 4c,d).

The inelastic ADCSs for $6s \rightarrow 6p_{1/2}$ (Fig. 5a) and for $6s \rightarrow 6p_{3/2}$ excitation (Fig. 5b) display a striking structure near the inelastic threshold that can be related to a $^3F^o$ resonance at the J-averaged energy E=1.62 eV [3, 22]. As for elastic scattering, the ADCS becomes strongly forward peaked as the scattering energy exceeds the close-to-threshold region. Recently, strong backward scattering close to the first inelastic threshold was also found in a merged-beam experiment for $3s \rightarrow 3p$ electron-impact excitation of Ar^{7+} [25]. Our results suggest that this phenomenon may be related to near-threshold resonances.

Comparison of the two subplots in Fig. 5 elucidates relativistic interactions through (i) the fine-structure split threshold for $6s \rightarrow 6p$ excitation and (ii) the deviation from

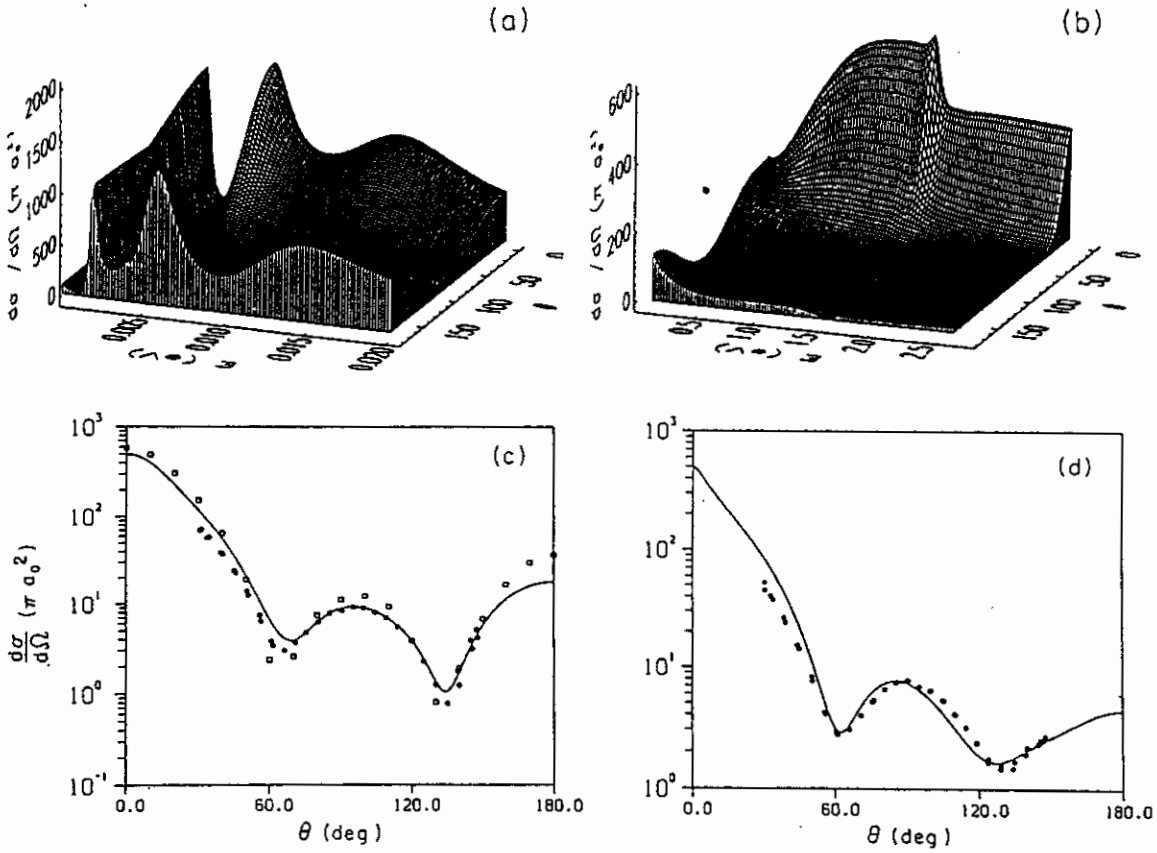

Figure 4: Angle-differential cross sections for elastic scattering. (a) E=0—20 meV; (b) E=0.1—2.7 eV; (c) E=1.4 eV; (d) E=1.6 eV. Experiment (relative): Ref. [22] (•). Theory: Dirac R-matrix calculation (Ref. [3]) (————); Ref. [4] (□).

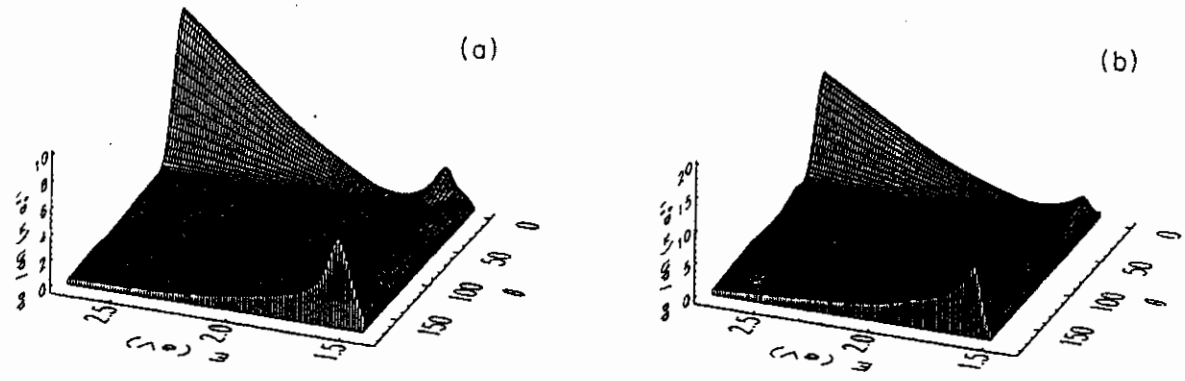

Figure 5: Angle-differential cross section (a) for $6s \rightarrow 6p_{1/2}$ and (b) for $6s \rightarrow 6p_{3/2}$ excitation.

the statistical branching ratio (=2), which is particularly striking for forward scattering at the highest shown energies and close to threshold. Note that without relativistic interactions, the two subplots would look alike.

3.5 Spin-Polarization Parameters

Cross sections for the scattering of unpolarized electrons extract only part of the information about the scattering process made available by our Dirac R-Matrix calculation through the spin-dependent scattering amplitudes [3]. In view of a complete description of the collision in terms of a maximal set of independent measurable quantities, which would be provided by a 'perfect scattering experiment' [18], we calculated the complete set of variables that parametrize the reduced spin density matrix for scattering of polarized electrons from unpolarized cesium atoms [15]. As an example, we show in Fig. 6 our results [15] for the seven 'generalized STU-parameters' [17] for $6s \rightarrow 6p_{1/2}$ excitation at E=1.6 eV that complement the ADCS in Fig. 4b. Comparison with the same parameters calculated for $6s \rightarrow 6p_{3/2}$ excitation (not shown here, cf. [15]) shows significant deviations for all seven variables. (This might not be surprising since we have already seen that the ADCSs strongly deviate from the statistical branching ratio.) Furthermore, relativistic interactions become apparent in comparison with the predictions $S_A[6s \rightarrow 6p_{1/2}] = -2S_A\ [6s \rightarrow 6p_{3/2}]$, $U_{xz} = U_{zx}$ and $T_x = T_y = T_z$ of a non-relativistic calculation [26].

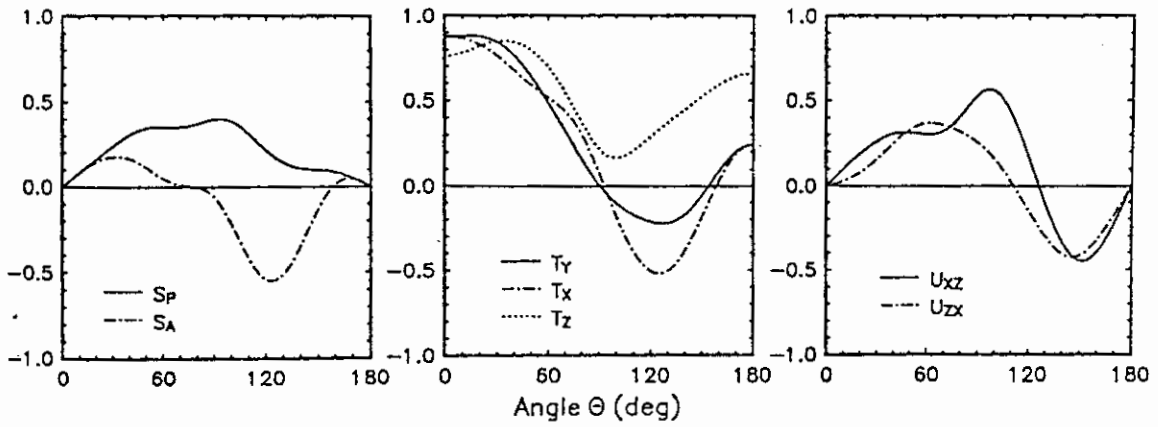

Figure 6: Generalized STU parameters for $6s \rightarrow 6p_{1/2}$ excitation at E=1.6 eV.

If both incident electrons and target are initially spin-polarized with parallel or antiparallel polarizations $\vec{P}_e$ and $\vec{P}_t$, parameters $A_{||}$ and $A_\perp$ can be determined according to $(\sigma_{\uparrow\uparrow} - \sigma_{\uparrow\downarrow}/(\sigma_{\uparrow\uparrow} + \sigma_{\uparrow\downarrow}) = A_{||,\perp}\ P_e P_t$, by measuring the ADCSs $\sigma_{\uparrow\uparrow}$ (for $\vec{P}_e \uparrow\uparrow \vec{P}_t$) and $\sigma_{\uparrow\downarrow}$ (for $\vec{P}_e \uparrow\downarrow \vec{P}_t$), where $\vec{P}_e$ and $\vec{P}_t$ either lie both in the scattering plane ($A_{||}$) or are perpendicular to it ($A_\perp$). Without relativistic effects one finds $A_{||} = A_\perp$, in sharp contrast to our numerical results (Fig. 7), that stress the dependence of sensitive spin-polarization parameters on relativistic interactions (most importantly on the spin-orbit coupling).

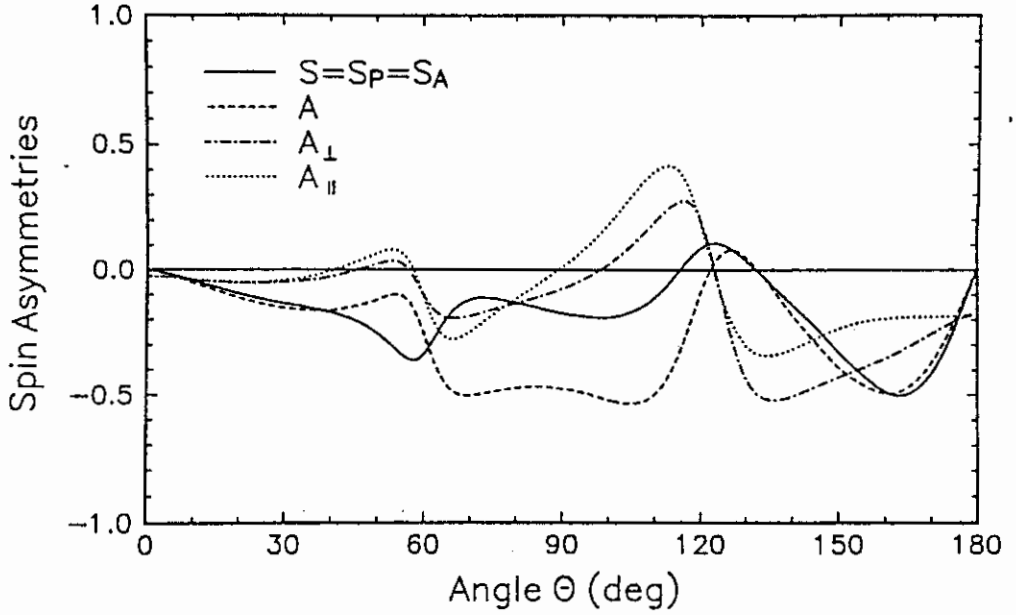

Figure 7: Sherman function S and spin-asymmetry parameters for elastic scattering of spin-polarized electrons from spin-polarized Cs atoms at E=1.6 eV.

3.6 Radiative Decay after Electron-Impact Excitation

The polarization characteristics of light emitted after electron-impact excitation of atoms can be expressed through 'integrated' (over the scattering angle of the unobserved projectile) 'Stokes parameters' (ISP). For electrons incident along the z-axis, for photons observed along the y-axis, and for emitted light intensities I(β) (for linear polarization at angle β to the z-axis) and $I_{+,-}$ (for circular polarization), these parameters are given by $\eta_1^y = (I(45°) - I(135°))/(I(45°) + I(135°))$, $\eta_2^y = (I_+ - I_-)/(I_+ + I_-)$, for transversely polarized electrons with spin polarization $\vec{P}_e = P_y\hat{e}_y$, and by $\eta_3^y = (I(0°) - I(90°))/(I(0°) + I(90°))$ for unpolarized incident electrons. For longitudinally polarized electrons ($\vec{P}_e = P_z\hat{e}_z$) and photons observed along the z-axis, for symmetry reasons only η_2^z can be nonzero [13].

¿From the scattering amplitudes of Ref. [3], we calculated the ISPs for the optical decay of impact-excited $6p_{1/2,3/2}$ states of Cs atoms [13]. The comparison of our Dirac-R-matrix results with experiment [27, 28, 29] and a previous semirelativistic Breit-Pauli R-matrix calculation [9] is quite satisfactory for some ISPs, in particular in view of the high sensitivity of the parameters and experimental uncertainities [13], while severe discrepancies exist for others (Fig. 8). We note that a nonrelativistic approach (i.e., the neglect of fine-structure splitting and all spin-dependent forces) would predict $\eta_1^y = 0$, whereas we find small values of the order of 1%.

4. CONCLUSIONS

We have used the Dirac R-matrix method as a vehicle for an accurate description of bound and low-lying continuous states of the e^- + Cs system in terms of a variety of parameters such as resonance positions and widths, cross sections, and spin- and light-polarizations. We find that core-polarization and relativistic effects are essential for the

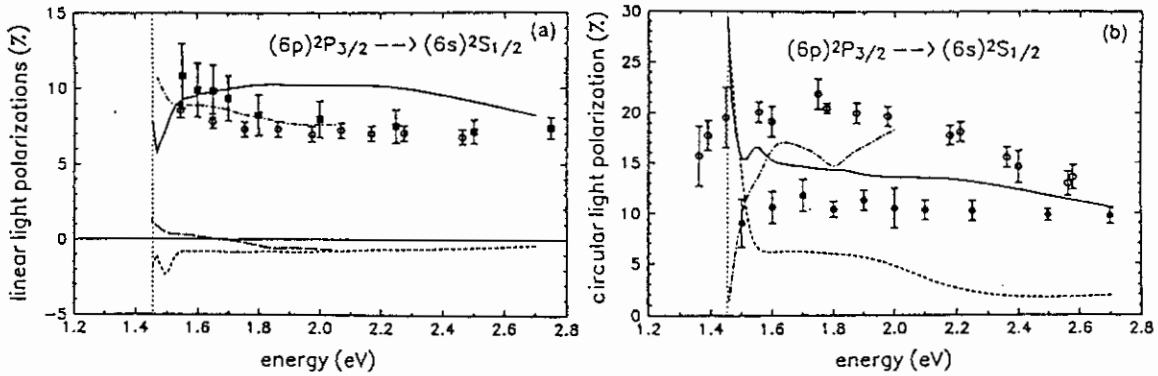

Figure 8: (a) Linear light polarizations for the optical transition $6p_{3/2} \rightarrow 6s_{1/2}$ in Cs after electron impact excitation: ————, present R-matrix calculation (Ref. [13]); for η_3^y; – – – – –, present result for η_1^y/P_y; — · — · — ·, Breit-Pauli result Ref. [9] for η_3^y; — — —, Breit-Pauli result for η_1^y/P_y. Experiment: (○), Ref. [27] for η_3^y; (■), Ref. [29]. (b) Circular light polarizations for the optical transition $6p_{3/2} \rightarrow 6s_{1/2}$ in Cs after impact excitation by spin polarized electrons. The individual curves are: ————, present result for η_2^y/P_y; – – – – –, present result for η_2^z/P_z; — · — · — ·, Breit-Pauli result for η_2^y/P_y. Experiment: (○), Ref. [27] for η_2^y/P_y; (●), Ref. [28] for η_2^z/P_z. The dotted line marks the excitation threshold of the $6p_{3/2}$ state.

detailed understanding of the scattering dynamics. In order to uniquely resolve existing discrepancies in the literature and to further test theoretical predictions, improved experimental investigations are highly desirable.

ACKNOWLEDGMENTS

This work was done in collaboration with David Norcross under the auspices of DOE. The generalized STU and Stokes parameters were calculated in collaboration with Klaus Bartschat. In the course of this work, I have benefited considerably from discussions with David, Klaus, Chris Greene, Michael Morrison, and many others I was lucky to meet at JILA.

References

[1] U. Thumm and D.W. Norcross, Phys. Rev. Lett. **67**, 3495 (1991); Phys. Rev. A**45**, 6349 (1992), and references therein.

[2] C.H. Greene, Phys. Rev. A**42**, 1405 (1990).

[3] U. Thumm and D.W. Norcross, Phys. Rev. A**47**, 305 (1993), and ref.s therein.

[4] E.M. Karule (1965); E.M. Karule and R.K. Peterkop (1965), as given in [1].

[5] P.G. Burke and J.F.B. Mitchell, J. Phys. B**6**, L161 (1973); **7**, 214 (1974).

[6] D.W. Norcross, Phys. Rev. Lett. **32**, 192 (1974).

[7] J.J. Chang, Phys. Rev. A**12**, 791 (1975); J. Phys. B**8**, 2327 (1975).

[8] N.S. Scott, K. Bartschat, P.G. Burke, O. Nagy, and W.B. Eissner, J. Phys. B**17**, 3775 (1984); **17**, L191 (1984).

[9] O. Nagy, K. Bartschat, K. Blum, P.G. Burke, and N.S. Scott, J. Phys. B**17**, L527 (1984).

[10] J.L. Krause and R.S. Berry, Comments At. Mol. Phys. **18**, 91 (1986).

[11] C.F. Fischer and D. Chen, J. Mol. Struct. **199**, 61 (1989).

[12] W.P. Wijesundera, I.P Grant, P.H. Norrington, and F.A. Parpia, J. Phys B**24**, 1017 (1991).

[13] K. Bartschat, U. Thumm and D. Norcross, J. Phys. B**25**, L641 (1992), and ref.s therein.

[14] K. Bartschat, private communication, and to be published.

[15] U. Thumm, K. Bartschat and D.W. Norcross, J. Phys. B**26**, 1587 (1993).

[16] I.I. Fabrikant, Opt. Spectrosc. (USSR) **53**, 131 (1982), and ref.s therein.

[17] K. Bartschat, Phys. Rep. **180** 1 (1989).

[18] B. Bederson, Comments At. Mol. Phys. **1**, 71 and **2**, 65 (1969).

[19] V.M. Borodin, I.I. Fabrikant and A.K. Kazansky, Phys. Rev. A**44**, 5725 (1991).

[20] P.J. Visconti, J.A. Slevin, and K. Rubin, Phys. Rev. A**3**, 1310 (1971).

[21] B. Jaduszliwer and Y.C. Chan, Phys. Rev. A**45**, 197 (1992).

[22] W. Gehenn and E. Reichert, J. Phys. B**10**, 3105 (1977).

[23] B. Stefanov, Phys. Rev. A**22**, 427 (1980).

[24] I.I. Fabrikant, J. Phys. B**19**, 1527 (1986).

[25] X.Q. Guo, et al., Phys. Rev. A**47**, R9 (1993).

[26] G.H. Hanne, Phys. Rep. **95**, 95 (1983).

[27] F. Eschen, G.F. Hanne, K. Jost, and J. Kessler, J. Phys. B**22** L455 (1989).

[28] P. Nass, M. Eller, N. Ludwig, E. Reichert, and M. Webersinke, Z. Phys. D**11** 71 (1989).

[29] S.T. Chen and A.C. Gallagher, Phys. Rev. A**17**, 551 (1978).